PHYSICAL REVIEW C, VOLUME 65, 034309

Highly deformed band structure in ^{57}Co

W. Reviol, D. G. Sarantites, R. J. Charity, and V. Tomov
Chemistry Department, Washington University, St. Louis, Missouri 63130

J. Dobaczewski
Institute of Theoretical Physics, Warsaw University, Hoza 69, PL-00681 Warsaw, Poland

D. Rudolph
Department of Physics, Lund University, S-22100 Lund, Sweden

R. M. Clark, M. Cromaz, P. Fallon, and A. O. Macchiavelli
Nuclear Science Division, Lawrence Berkeley National Laboratory, Berkeley, California 94720

M. P. Carpenter and D. Seweryniak
Physics Division, Argonne National Laboratory, Argonne, Illinois 60439

(Received 7 September 2001; published 14 February 2002)

Rotational bands have been found in ^{57}Co using the ^{28}Si(^{32}S,3p) reaction at 130 MeV. The bands, extending the mass 60 region of large deformation down to $Z=27$, are signature-partner sequences. Their quadrupole moments are similar to those of bands in the neighboring nuclei. The features of the new bands are described by Skyrme Hartree-Fock calculations favoring a configuration assignment with one neutron and one proton excited in the respective $1g_{9/2}$ intruder orbital. An attempt to describe the magnetic ($M1$) properties of the signature-partner structure is also presented.

DOI: 10.1103/PhysRevC.65.034309 PACS number(s): 27.60.+j, 23.20.Lv, 21.60.Cs

I. INTRODUCTION

In recent years, considerable effort has been devoted to explore the island of exotic shapes in the mass 60 region. Rotational bands associated with a highly deformed ($\beta_2 > 0.3$) or superdeformed ($\beta_2 \sim 0.45$) quadrupole shape have been found there, specifically in isotopes of Zn, Cu, and Ni (see, e.g., Refs. [1–4]). The underlying configurations are explained by particle-hole excitations across the $N=Z=28$ shell gap in which the shape-driving $N_0=4$ $1g_{9/2}$ intruder orbital plays a pivotal role. Remarkably, these band structures can be and have been approached with various models (classical and Monte Carlo shell models [2,5], Nilsson-Strutinsky and relativistic mean field approaches [6], and large-scale Hartree-Fock calculations [7]) and a consistent picture—the one mentioned above—has emerged. Since several theoretical approaches can be confronted with new experimental data, this nuclear region is of broad interest for both experimentalists and theorists.

The rotational sequences in the mass 60 region serve also as a contrast to those in the ‘‘traditional’’ regions of superdeformation at masses 80, 150, and 190 because of the occurrence of a so-called smooth band termination [8]. Such an effect is expected in these relatively light nuclei, which have a smaller number of valence particles than the heavier nuclei and thus exhaust the angular momentum content of their single-particle configurations faster than the heavier nuclei (but still gradually). Interestingly, despite the expected loss of collectivity the bands remain well deformed over the entire spin range.

In the present work, the picture of particle-hole excitations across the shell closure is investigated further by studying the nucleus ^{57}Co. We have found in this nucleus a highly deformed band structure consisting of two signature-partner sequences. This finding extends the mass 60 region of deformation below the $Z=28$ shell gap. Furthermore, it represents one of the first cases for a band structure in an odd-mass nucleus in the mass 60 region (the previously known cases are mostly even-even or odd-odd nuclei). The band structure in ^{57}Co is compared with results from the Skyrme Hartree-Fock calculations outlined in Ref. [7]. A preliminary account of the present work can be found in Ref. [9].

II. EXPERIMENT AND DATA REDUCTION

The experiment was carried out at the Argonne Tandem Linac Accelerator System. High-spin states in ^{57}Co were populated in the ^{28}Si(^{32}S,3p) fusion-evaporation reaction at a beam energy of 130 MeV. The target enriched to 99% in ^{28}Si had a surface density of 0.5 mg/cm^2 and was supported by a 1 mg/cm^2 Au layer facing the incoming beam. The γ rays from the reaction were detected by the Gammasphere array [10], which contained 78 high-purity Ge detectors in BGO Compton-suppression shields. The Hevimet collimators were removed to obtain γ-ray sum energy and fold information per event. Thirty Ge-BGO modules of the six most forward rings were replaced by a shell of 30 neutron detectors [11]. The neutron shell served for the purpose of selecting one and two neutron evaporation channels and was used for the first time in Gammasphere [12]. The evaporated charged particles were detected simultaneously with the 4π CsI-array Microball [13]. The event trigger required the presence of four or more Ge detectors in prompt coincidence with each other and in anticoincidence with their suppressor shields or a minimum of two "clean" Ge detectors and a neutron detector. Under this condition, a total of about 700 million events were collected during two days of running time.

In the off-line analysis, the γ-ray data were sorted according to individual detected exit channels. Gates were placed on the identified charged particles (and/or neutrons). Contaminants in these gates resulting from particles that escaped detection were sharply reduced by applying the total energy plane selection method of Ref. [14]. The Doppler-shift correction for the γ-ray energies was based on the velocity vectors of the recoiling nuclei which were reconstructed from the momentum vectors of the compound nucleus and the evaporated particles detected. A γ-ray energy dependent recoil velocity was applied to compensate for the slowing down of the recoils in the target, and, thus, further sharpen the energy spectra. Finally, E_γ-E_γ matrices and E_γ-E_γ-E_γ cubes of γ-ray coincidence events were created.

The $3p$ evaporation channel was estimated to account for about 12% of the total fusion cross section, representing one of the strongest channels. In the $3p$ channel selected matrix, only measurable contaminants from the $4p$ and $3pn$ channels were found. These remainders of contaminant exit channels were removed by subtracting the normalized portions of background matrices gated by those contaminants. The normalization factors used were 1.298 ($4p$) and 1.957 ($3pn$), indicating that the approximate efficiency for the detection of one proton and one neutron was 75% and 33%, respectively. In order to simulate the reduced energy resolution in the background matrices, the proper number of undetected particles were excluded from the recoil correction procedure.

The γ-ray multipolarities were inferred from a directional correlation (DCO) analysis. The data from adjacent rings of Gammasphere were summed together to produce a channel selected $E_\gamma^{\theta_1}$-$E_\gamma^{\theta_2}$ matrix with θ_1 and θ_2 corresponding to average detector angles of 142.7° (backward) and 90.0° with respect to the beam axis. An intensity ratio

$$R_{DCO}=\frac{I_{\gamma_2}^{\theta_1}(\text{gate}_{\gamma_1}^{\theta_2})}{I_{\gamma_2}^{\theta_2}(\text{gate}_{\gamma_1}^{\theta_1})} \tag{1}$$

was introduced for the analyzed transition γ_2, where the peak areas obtained for γ_2 at θ_1 and θ_2 were corrected for the relative efficiencies of the detectors at these angle positions. For the gating transition γ_1, only peaks of stretched quadrupole character were considered. The type of each transition was restricted to either stretched dipole ($M1$ or $E1$) or quadrupole ($E2$) radiation or the appropriate $E2+M1$ mixing of these multipolarities. The shortcomings of this method are its inability to determine the degree of mixing and the disadvantage that $E2$ and nonstretched dipole ($\Delta I=0$) transitions are practically indistinguishable.

For transitions of known multipolarity between low-spin states in ^{58}Ni (a nucleus with a significant population in the present experiment), it was found that $R_{DCO}\simeq 0.8$ if γ_2 is a stretched and rather pure dipole transition and $R_{DCO}\simeq 1.1$ if γ_1 and γ_2 are of the $E2$ type. The reference value of 1.1 is, however, a lower limit estimate for $E2$ transitions. At high spins, the angular-distribution attenuation coefficients are known to be considerably larger than those at low spins (see, e.g., Ref. [15], Fig. 5) and this increases the R_{DCO} value up to 1.6. The value $R_{DCO}\simeq 0.8$ for dipole transitions, on the other hand, may be taken as a representative value for the bulk of dipole transitions, which are in this nuclear region $M1$ in character and presumably contain an admixture but of unknown degree.

A residual Doppler-shift analysis [16] was performed to obtain transition quadrupole moments for the level structures of interest. For this purpose, the channel selected γ-ray data were sorted according to five different angle groups of the Gammasphere array with average angles of 72.9°, 90.0°, 107.1°, 127.2°, and 151.2° with respect to the beam axis. Subsequently, fractional Doppler shifts $F(\tau)$ of the crucial γ-ray transitions were extracted.

III. RESULTS

Figure 1 shows the main part of the level scheme for ^{57}Co. The spin and parity assignments for the states up to the first $19/2^-$ state are adopted from previous work [17]. The spins for the higher-lying states are assigned on the basis of the DCO analysis described above. In addition, it is *assumed* that levels decaying predominantly to known negative-parity levels have themselves negative parity. The transitions with energies given in parentheses are tentatively placed due to their weakness or the presence of unresolved doublets or multiplets.

The level structure at low spin is very complex and probably reflects the many possibilities of single-particle excitations in this nucleus [17]. Above spin $I=25/2$, however, a band structure develops. This structure is formed by two sequences of electric quadrupole ($E2$) transitions, labeled (h) and (i), which are interlinked at the bottom. Sample coincidence spectra for this structure are shown in Fig. 2. The spectra in the two upper panels are obtained from sums of coincidence gates placed on in-band transitions. All band members and the interband transitions are labeled by their energies in keV. A spectrum gated by the 731 keV interband transition is presented in the bottom panel, confirming the reported coupling of bands (h) and (i) as well as their main decay-out branch ($E_\gamma=2347$ and 2799 keV). The 2292 keV transition in band (i) is a member of a multiplet (with the strongest component being the 2290 keV $17/2^-\rightarrow 13/2^-$ transition). Its placement as a band member is reasonable because gates on band (i) transitions enhance a 2292 keV γ ray considerably as compared to the coincidence spectra gated by band (h) transitions.

Figure 3 shows the DCO ratios according to expression (1) for transitions in ^{57}Co. The distinction between stretched $E2$ transitions and dipole or mixed transitions is made by means of the R_{DCO} reference value obtained for $E2$ low-spin transitions in a neighboring nucleus (cf. Sec. II). The transitions of the high-spin band structure are highlighted by triangles, while for the majority of the transitions another set of symbols (circles) is used. The dipole character of all inter-

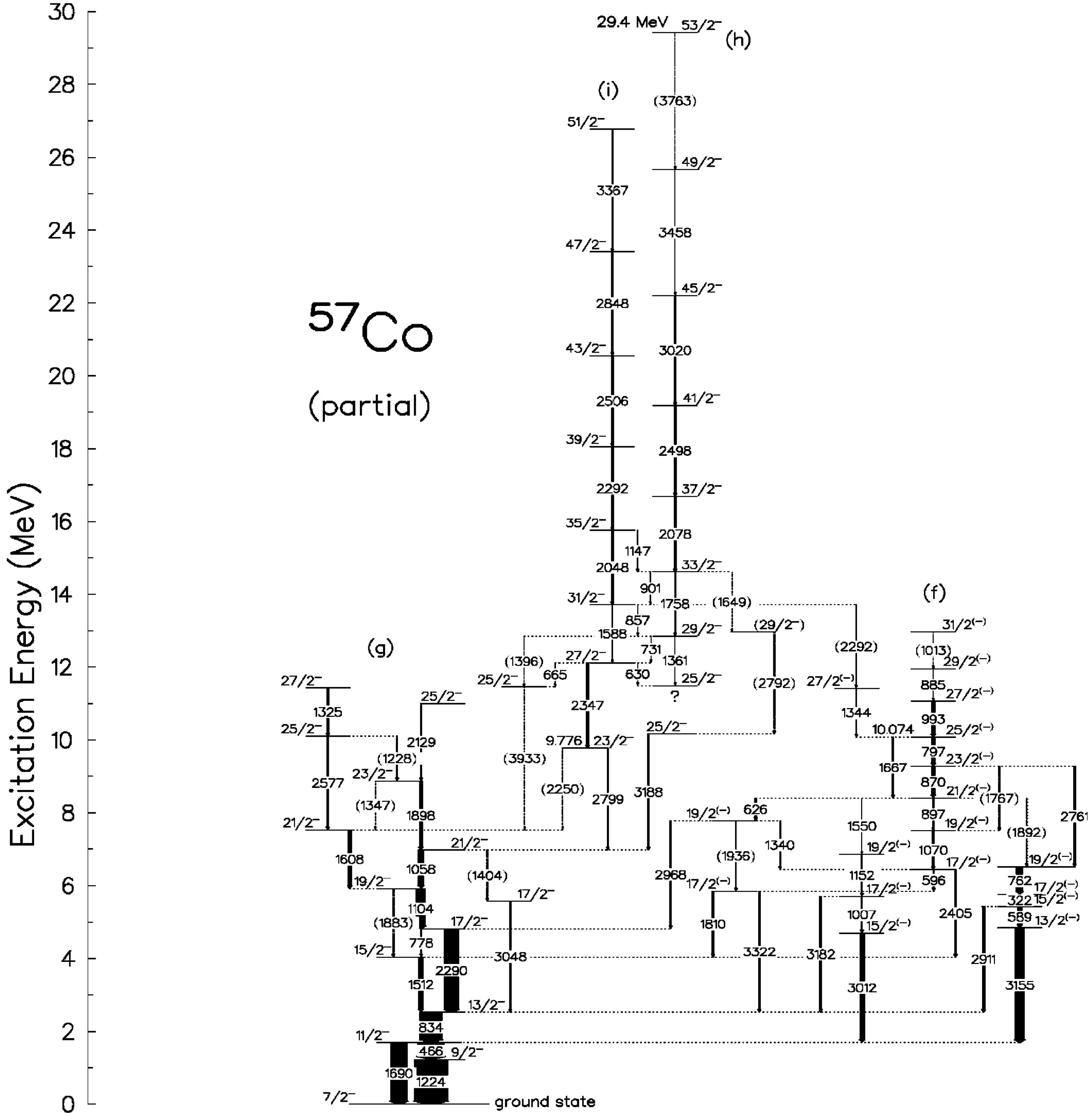

FIG. 1. Partial level scheme for ^{57}Co showing the high-spin band structure, (h) and (i), and the level sequences fed by this structure, (f) and (g). Transitions are labeled by their γ-ray energies in keV; typical uncertainties are 1–2 keV. The arrow widths represent the relative intensities of the transitions. The question mark below the $25/2^-$ "bandhead" state indicates that the decay of this level has not been observed. Two lower-lying states with spin and parity $23/2^-$ and $25/2^{(-)}$, respectively, are also labeled by their excitation energies in MeV to ease the description of the scheme.

band transitions and the $E2$ character of most of the in-band transitions are firmly established from the DCO ratios. For the highest band members the multipolarity cannot be determined from the present data because of the weak intensities involved. Nevertheless, their assignments are likely because of the rotational-like character of these sequences. For the lowest in-band transition, with $E_\gamma = 1361$ keV, no DCO ratio could be extracted either. The spin assignments for its initial and final state are determined by the multipolarities of the two transitions with $E_\gamma = 630$ and 731 keV which bypass the 1361 keV transition. The interband transitions are proposed to be of $M1$ type, by analogy with band structures in ^{62}Zn [4] and ^{65}Zn [18]. Consequently, the bands (h) and (i) are viewed as signature-partner bands.

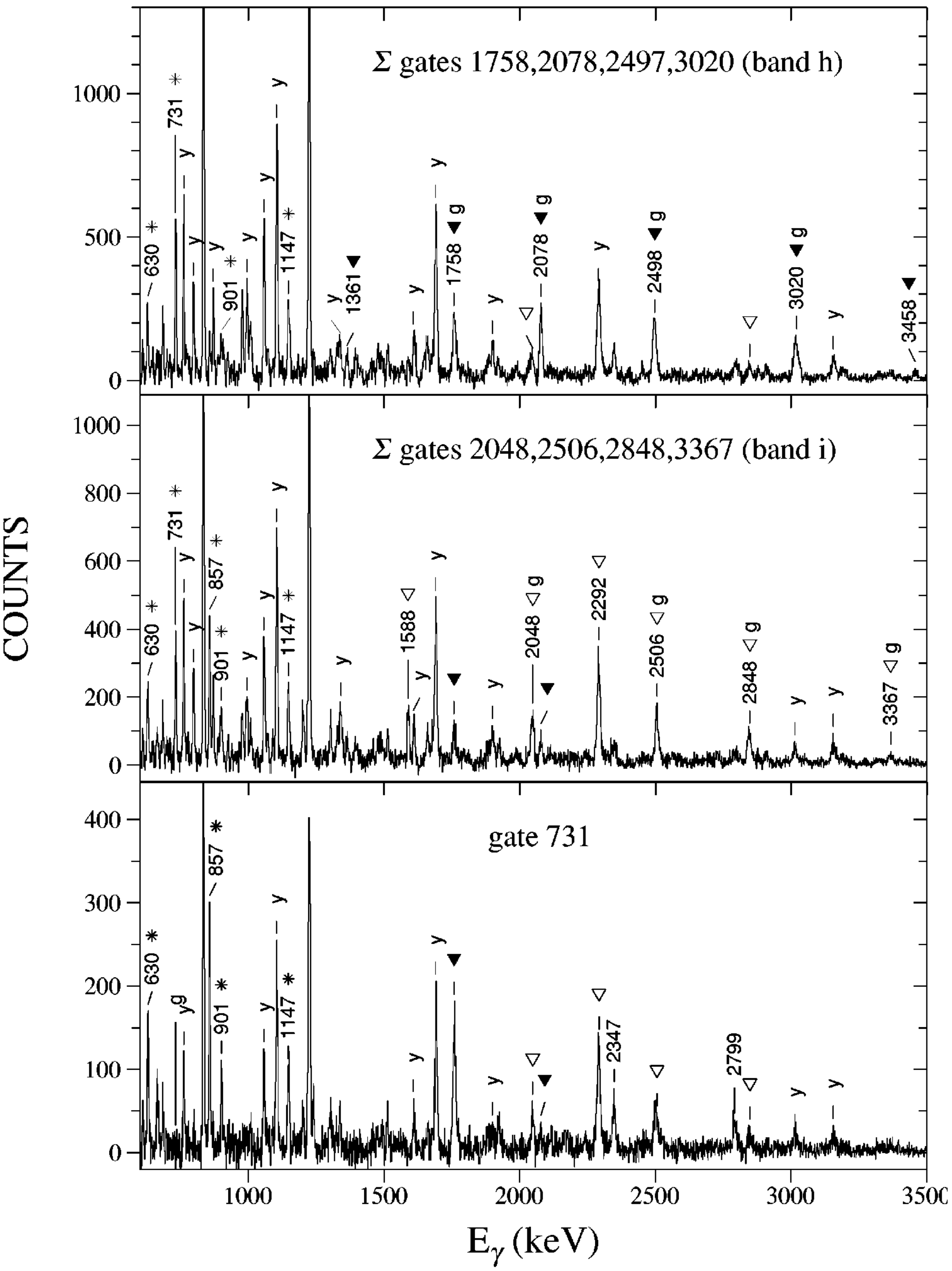

FIG. 2. Coincidence spectra for the high-spin band structure in ^{57}Co. Gating transitions are given in the figure and labeled by the symbol "g." The transitions in the sequences (h) and (i) are highlighted by filled and open triangles, respectively, and the signature-partner linking transitions by asterisks. The most intense γ rays and those labeled "y" are transitions between lower-lying states in ^{57}Co near the yrast line.

A general observation from Fig. 3 is that a number of transitions between spherical states with γ-ray energies of about 1000–2000 keV are admixtures, i.e., of $E2/M1$ type with a spin change $\Delta I = 1$. For example, the 1058, 1608, and 1898 keV transitions belong to this category. The spin-parity assignment of $21/2^-$ for the initial state of the 1058 keV transition is supported by the presence of a weak $E_\gamma = 1404$, 3048 keV sequence bypassing the yrast transitions of level structure (g). These two γ rays are proposed to be $E2$ transitions leading to the maximum spin change, where the $E2$ assignment for the 1404 keV transition is consistent with the lower limit estimate for R_{DCO} shown in Fig. 3 (no DCO ratio could be measured for the 3048 keV γ ray). The proposed absence of any parity change in the level scheme of Fig. 1 is a particularly safe assumption for the structure labeled (g). For the other structures, no reason is found to consider a parity change. However, the parity assignments for the structure (f) are considered to be less certain than those for the rest of the level scheme and therefore are given in parentheses.

In one case, the relative population of levels has been used to assign spins to the lower-lying states rather than the available multipolarity information: The 2799 and 2250 keV γ rays are proposed to be $E2/M1$ ($\Delta I = 1$) transitions, resulting in a spin-parity assignment of $23/2^-$ for their initial state at 9.776 MeV. The value $R_{DCO} = 1.341(68)$ for the 2799 transition favors an $E2$ or a $\Delta I = 0$ assignment and rules out an $E1$ assignment, whereas no DCO ratio could be measured for the 2250 keV transition. However, if the spin of the 9.776 MeV level would be one unit higher than the value proposed (i.e., for an $E2$ assignment) then the state would be yrast. This scenario would be inconsistent with the level

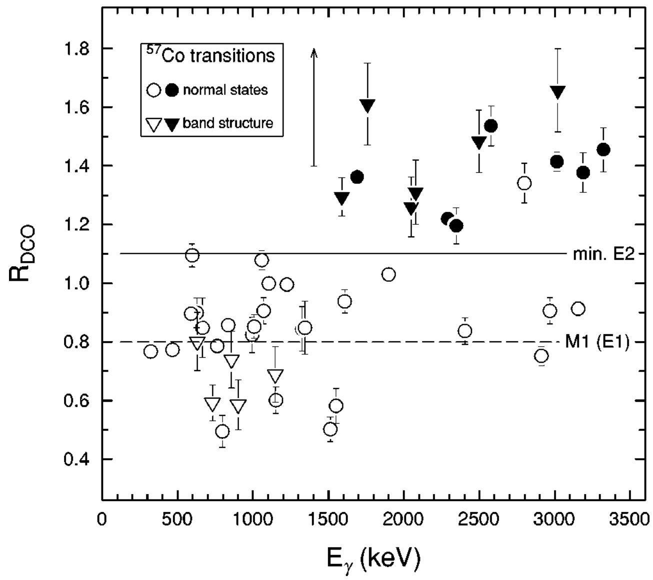

FIG. 3. DCO ratios as described in the text versus γ-ray energy. Dipole and quadrupole transitions are represented by open and filled symbols, respectively. For the 1404 keV transition, only a lower limit estimate is given. The straight lines indicate the R_{DCO} reference values obtained for dipole and $E2$ low-spin transitions in a neighboring nucleus. The latter value represents a minimum value for $E2$ transitions (see text).

scheme since the 10.074 MeV state at spin 25/2 in the level structure (f), which decays by the 797 and 1667 keV transitions, is more strongly populated than the 9.776 MeV level. A decay of the 9.776 MeV level by $\Delta I=0$ transitions is deemed to be unlikely for a state located rather high in the level scheme. In addition to the arguments presented above, it should be mentioned that only the spin 23/2 assignment for the state at 9.776 MeV is consistent with the spin assignments made for the 2347 keV decay-out transition and the other (weaker) decay-out branches for the high-spin bands. Among those branches is the $E_\gamma=1344$, 2292 keV sequence for which DCO ratios are measured.

The decay intensity of the signature-partner bands in ^{57}Co is spread over several pathways linking them with both the level structures (f) and (g), the latter one being favored. The observed decay-out transitions account for ~80% of the intensity of the bands. As indicated in Fig. 1, the decay of the weakly populated $25/2^-$ "bandhead" state is not observed. Therefore, it is important to ensure that in the present level scheme no significant transitions are missing and the following check of the spin assignments is in order.

Figure 4(a) shows the intensity patterns of the yrast sequences over a large spin range. Indeed, the crossing of these patterns (between spins 27/2 and 29/2) is supportive for the sequence of γ-ray transitions near the yrast line and their corresponding spin assignments. The branching ratio for the decay intensity of the signature-partner band between interband ($M1$) and in-band ($E2$) transitions is shown in Fig. 4(b). Conclusions from this pattern are drawn in Sec. IV.

The possibility of a proton decay near the bottom of the ^{57}Co bands, similar to the case of, e.g., ^{58}Cu [2], has been also investigated and the result is negative. For this particular investigation, the γ-ray events associated with ^{57}Co and ^{56}Fe have been "mixed" and a combined set of triples coincidence data has been analyzed using a double-gating procedure with a gating transition (or a list of gating transitions) in each nucleus. No evidence for coincidence relationships between transitions of band (h) or band (i) in ^{57}Co and yrast transitions in ^{56}Fe has been found in this analysis. However, because of limited statistics the presence of a weak proton-decay branch corresponding to $\lesssim 20\%$ of the intensity of the bands cannot be ruled out. The high-spin band structure in ^{57}Co is considered to be well linked to the low-spin part of the level scheme.

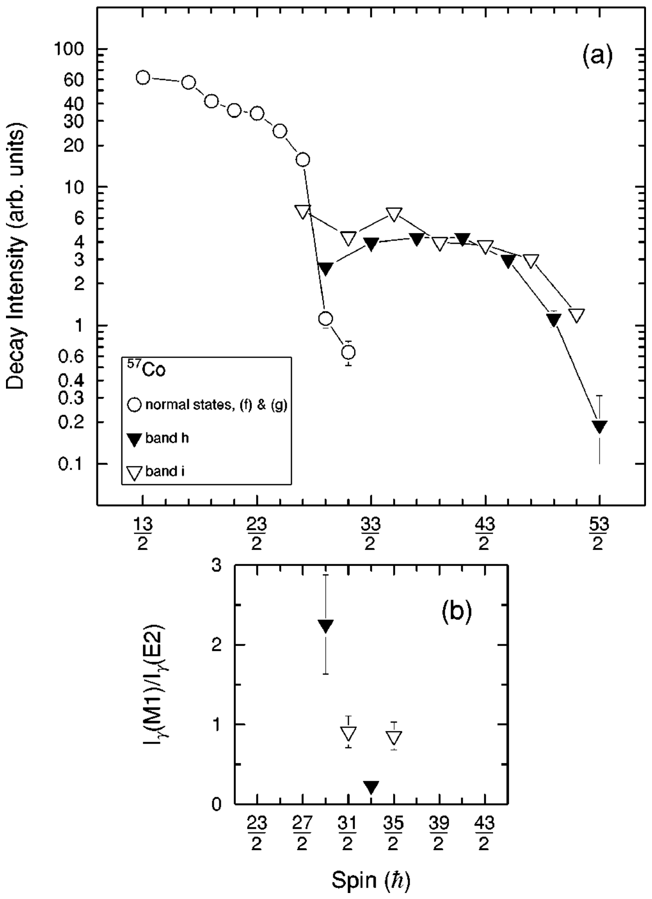

FIG. 4. (a) Relative intensities of yrast and near-yrast transitions as a function of initial spin. (b) Branching ratios $I_\gamma(M1)/I_\gamma(E2)$ versus spin for the interband and in-band transitions of bands (h) and (i).

The collective character of bands (h) and (i) is inferred from their average transition quadrupole moments measured with the thin-target Doppler-shift attenuation method [16]. Figure 5 shows the fractional Doppler shifts $F(\tau)$ for each band and, for comparison, some transitions between lower-spin states (1058, 1104, 1690, 2290, 2347, 2799, and 3155 keV). The highest band members for which $F(\tau)$ values could be extracted are the $45/2^- \rightarrow 41/2^-$ (band h) and $47/2^- \rightarrow 43/2^-$ (band i) transitions. The fitted curves are calculated using the side feeding model of Ref. [19], the measured intensity profiles of bands (h) and (i), and for the slowing down in the target the stopping powers provided by the

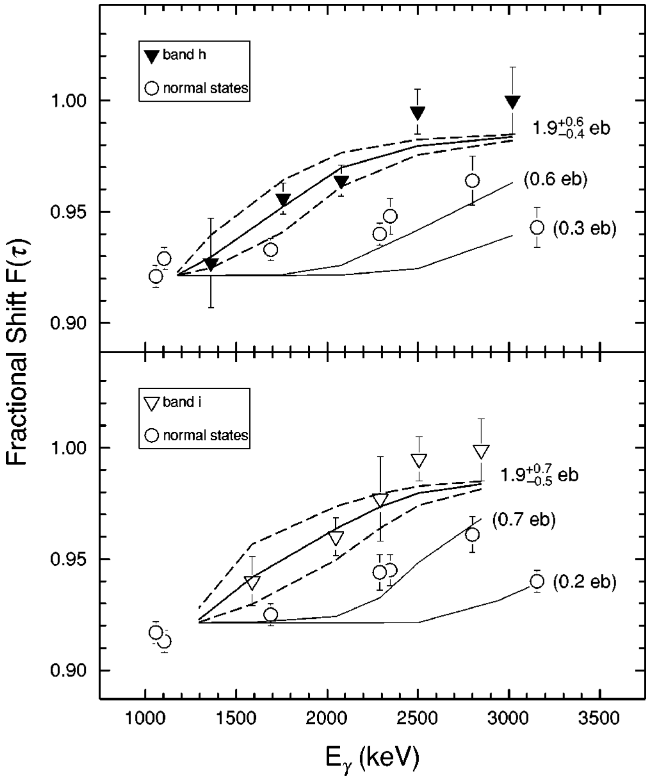

FIG. 5. Fractional shift $F(\tau)$ as a function of γ-ray energy. Triangles represent the data for the high-spin bands, and circles the data for some representative low-spin transitions in the same spectral range. Calculated $F(\tau)$ curves with different values Q_t are shown for comparison. The dashed curves among them represent 1σ deviations from the best fit for the high-spin bands. The $F(\tau)$ curve for 0.2 eb in the bottom panel is calculated using a slightly larger spin range than for the other curves.

code TRIM [20]. The best fits are obtained for transition quadrupole moments $Q_t = 1.9^{+0.6}_{-0.4}$ eb and $1.9^{+0.7}_{-0.5}$ eb for bands (h) and (i), respectively. The quoted errors represent a 1σ deviation from the best fit but exclude the systematic errors associated with the stopping powers which are smaller.

The transition quadrupole moments measured for bands (h) and (i) are significantly larger than the Q_t values appropriate for the set of lower-spin transitions, which are also given in Fig. 5. The Q_t value of 1.9 eb corresponds to a quadrupole deformation $\beta_2 = 0.39$ for an axial shape. However, the deformation is rather $\beta_2 > 0.39$ since the deformed shape is expected to be somewhat triaxial with a positive value of the γ parameter, as mentioned in the following section. For example, by taking $\gamma = 5°$ one obtains $\beta_2 = 0.41$. It is also interesting to notice that the Q_t values for the bands in ^{57}Co are comparable with those measured for the high-spin bands in neighboring Ni and Cu nuclei, e.g., in ^{56,58}Ni [3,21] and ^{58}Cu [2]. In summary, the new bands in ^{57}Co represent a highly deformed shape of the ^{57}Co nucleus.

IV. DISCUSSION

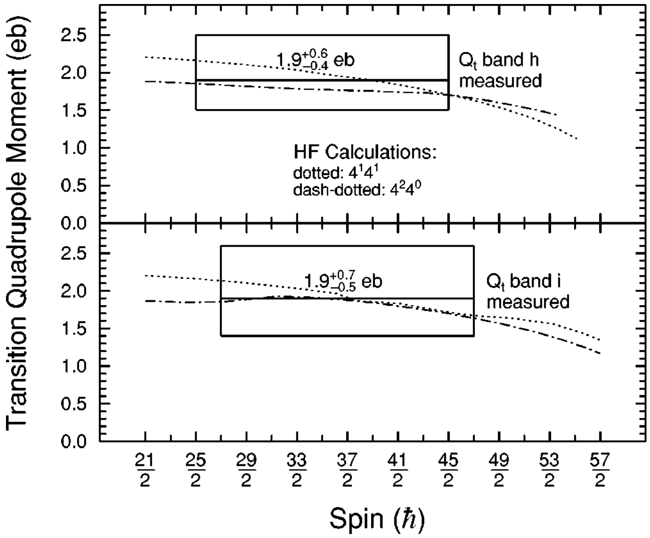

FIG. 6. Comparison between calculated and measured transition quadrupole moments for the bands in ^{57}Co. The boxes represent the average Q_t values (with uncertainty) measured in a certain spin range as described in the previous section.

Properties of the high-spin bands in ^{57}Co are compared with results of the cranked Hartree-Fock (HF) calculations performed by using the HFODD (v1.75r) computer code [22], with the Skyrme SLY4 [23] effective interaction, and no pairing (see Ref. [7] for details). The configuration assignment proposed for the ^{57}Co high-spin bands is guided by (i) parity considerations, (ii) quadrupole moments, (iii) configuration crossings judged by, e.g., the behavior of the $\mathfrak{J}^{(2)}$ moment of inertia as a function of rotational frequency, and (iv) degeneracy of the signature-partner configurations. The configurations are described by the notation 4^n4^p, where n and p are the numbers of occupied $N_0 = 4$ unique parity Routhians originating from the $1g_{9/2}$ intruder orbital. The remaining particles occupy negative-parity Routhians, and hence the total parity of the ^{57}Co configurations is $\pi = -(-1)^{n+p}$.

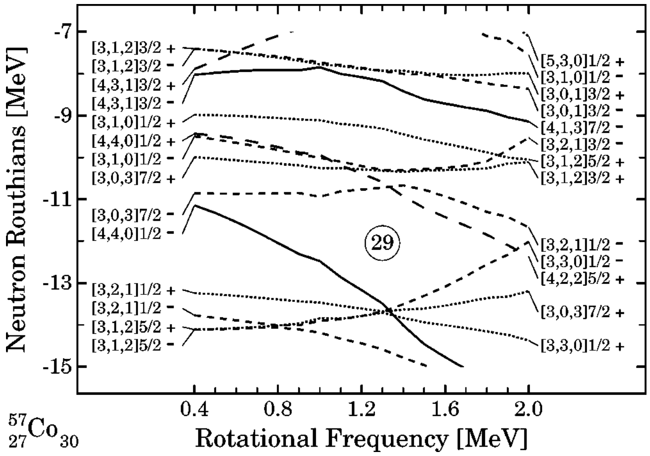

FIG. 7. Neutron single-particle Routhians calculated for the 4^14^1 configuration in ^{57}Co ($N = 30$). For the negative parity, all states corresponding to the Routhians below the $N = 29$ gap are occupied, while the 30th neutron occupies the $[303]7/2(-i)$ Routhian at low frequencies and the $[310]1/2(-i)$ Routhian at high frequencies. The latter one is, as indicated in the figure, at $\hbar\omega = 2$ MeV dominated by the $[321]1/2(-i)$ Nilsson state.

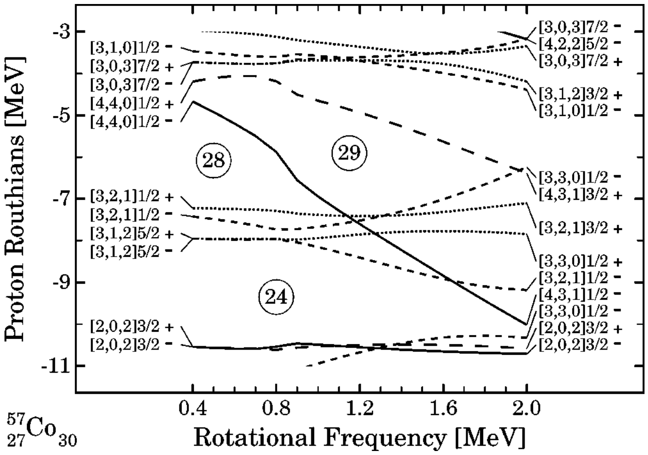

FIG. 8. Proton single-particle Routhians calculated for the 4^24^0 configuration in ^{57}Co ($Z=27$). For the negative parity, nearly all states corresponding to the Routhians below the $Z=28$ gap are occupied. The only exceptions are the holes in the $[321]1/2(-i)$ Routhian at low frequencies and the $[312]5/2(-i)$ Routhian at high frequencies. The latter one is at $\hbar\omega=2$ MeV dominated by the $[330]1/2(-i)$ Nilsson state.

The bands in ^{57}Co have most likely negative parity, see Fig. 1. Therefore, the discussion is restricted to the lowest negative-parity configurations, that is, only intruder configurations of the 4^24^0 and 4^14^1 types are considered. The negative-parity configurations without intruder content (4^04^0) are ruled out by the large transition quadrupole moments measured, and those with $n<p$ are unlikely in a nucleus with $N=Z+3$.

The measured Q_t values do not allow one to distinguish also between the two intruder configurations. This is shown in Fig. 6 where the measured average Q_t values and the transition quadrupole moments calculated for the 4^24^0 and 4^14^1 configurations as a function of spin are compared with each other. The spin range shown for each Q_t value is situated between the bandhead and the highest band member for which an $F(\tau)$ value could be extracted. The largest difference between the theoretical curves is in the spin range near the bandhead but the present measurement is not sensitive to such a difference nor to a noticeable reduction of the quadrupole moment at very high spin. The calculations also show a *slow* migration of the nuclear shape into the nonaxial, noncollective sector with increasing spin and rotational frequency. For example, for the 4^14^1 configuration, the γ deformation parameter is calculated to increase from 3° at the bandhead to 26° at the top of the structure in an exponential fashion. The γ values for the 4^24^0 configuration are overall smaller. In the following paragraphs we try to reach a conclusion as to which of the two options (4^24^0 or 4^14^1) is most suitable to describe the bands in ^{57}Co.

Figures 7 and 8 show the neutron single-particle Routhians for the 4^14^1 configuration and the proton single-particle Routhians for the 4^24^0 configuration, respectively. These energy levels are labeled by standard Nilsson quantum numbers and a sign (±) representing the signature quantum number $r=\pm i$. Given in the figures are the dominant components of the HF wave functions at low (left set) and high (right set) rotational frequencies. The wave functions change with frequency because of the strong Coriolis mixing. The agreement between calculated and measured quadrupole moments (Fig. 6) indicates that the present calculations provide a good description for the bands in ^{57}Co.

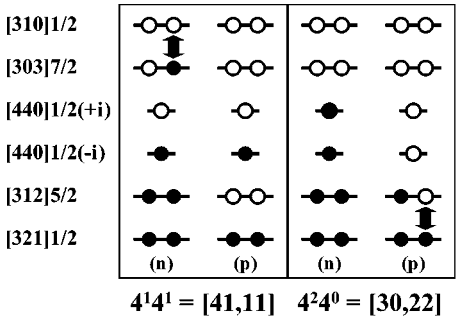

FIG. 9. Schematic diagram illustrating the occupied single-particle Routhians (full circles) for the 4^14^1 (left) and 4^24^0 (right) configurations in ^{57}Co. The Nilsson labels shown at the left represent the dominating components of the HF wave functions calculated at low frequencies; these can be different at high frequencies (cf. Figs. 6 and 7). At the bottom, the discussed configurations are also given in the notation of Ref. [6]. The arrows indicate the crossings of the Routhians discussed in the text.

Since the high-spin sequences in ^{57}Co form a signature-partner structure, and the positive-parity intruder states are calculated to be strongly split in energy, the observed bands must correspond to occupying the lowest-lying pair of negative-parity signature-partner states. In the case of the 4^14^1 configuration, the two bands are due to the occupation

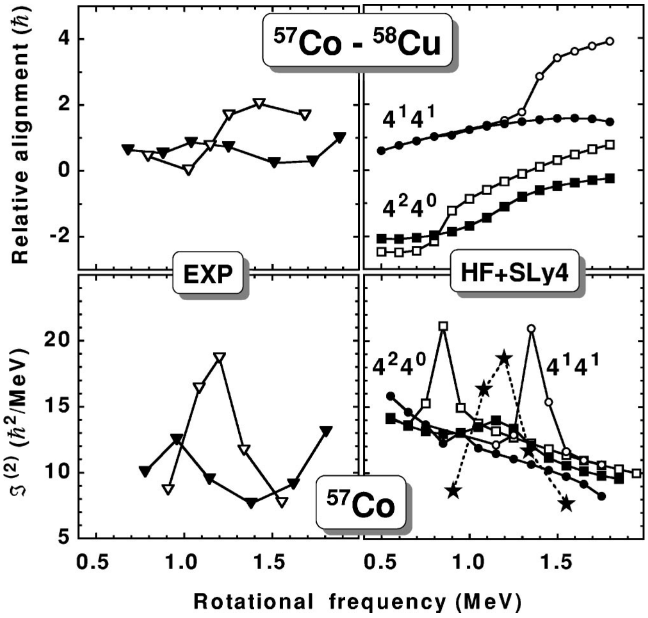

FIG. 10. Relative spin alignments between the bands in ^{57}Co and ^{58}Cu (top) and dynamic moments of inertia for the bands in ^{57}Co (bottom) as a function of rotational frequency. Data obtained from experiment (left) are compared with the results of the HF +SLY4 calculations (right). For the $r=+i$ band, the experimental values of $\Im^{(2)}$ are repeated in the bottom right panel (stars) to ease the comparison.

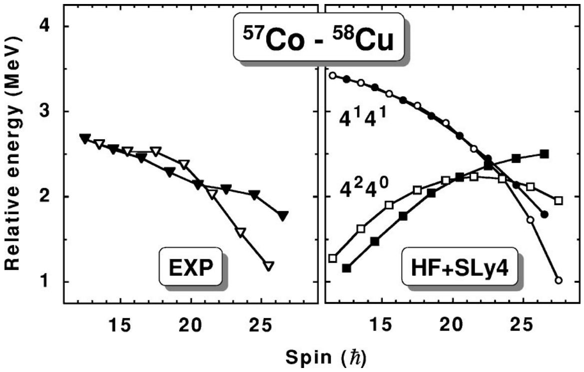

FIG. 11. Relative energies between the high-spin bands in ^{57}Co and ^{58}Cu as a function of spin. Experimental (calculated) values are shown at left (right).

of one of the $\nu[303]7/2(\pm i)$ states by the 30th neutron [24]. At the same time, the pair of protons is put in the $\pi[321]1/2(\pm i)$ states and kept there in the entire range of rotational frequencies. Around $\hbar\omega = 1.3$ MeV, the $\nu[303]7/2(-i)$ Routhian is crossed by the $\nu[310]1/2(-i)$ state. This perturbs one of the signature-partner bands (the one for the $r = +i$ signature), and leads to a bump in the corresponding $\mathfrak{I}^{(2)}$ moment of inertia, see below.

In the case of the 4^24^0 configuration, the two signature-partner bands are obtained by putting the 27th proton in one of the $\pi[312]5/2(\pm i)$ states. Around $\hbar\omega = 0.9$ MeV, the $\pi[312]5/2(-i)$ Routhian is crossed by the $\pi[321]1/2(-i)$ level, which also gives a bump in the $\mathfrak{I}^{(2)}$ moment.

Therefore, in ^{57}Co one has two natural candidate configurations in which crossings occur in the $r = +i$ bands. The diagram in Fig. 9 summarizes the occupations of single-particle states in both scenarios (4^14^1 and 4^24^0). The discussed crossings of Routhians are highlighted by arrows shown in the diagram.

In order to evaluate further the level of agreement between the two theoretical scenarios and the experimental data, we compare in Figs. 10 and 11 the following parameters: the measured and calculated $\mathfrak{I}^{(2)}$ moments for ^{57}Co versus rotational frequency, the corresponding spins with respect to the superdeformed band in ^{58}Cu (relative alignment), and, separately, the relative energies between the levels in the ^{57}Co and ^{58}Cu bands. The superdeformed band in ^{58}Cu [2,25] is chosen as a "reference," since alignments are absent in this structure as indicated by a "flat" $\mathfrak{I}^{(2)}(\hbar\omega)$ behavior. However, to facilitate the comparisons two artificial transitions of 3641 and 4128 keV are added to it at the top, thus covering the frequency range of the ^{57}Co bands.

The values for the relative alignment, shown in the top panels of Fig. 10, are reproduced by the 4^14^1 configuration, while those obtained for the 4^24^0 case are too small by about two units. It should be pointed out that predictions for the relative alignment are fairly robust, because they mainly depend on the occupations of the $1g_{9/2}$ intruder orbitals that carry most of the alignment [7]. As shown at the bottom of Fig. 10, the experimental $\mathfrak{I}^{(2)}$ moment of the $r = +i$ band in ^{57}Co exhibits an irregularity around $\hbar\omega = 1.2$ MeV indicative of a configuration crossing. This crossing frequency is more closely approached by the bump of the $\mathfrak{I}^{(2)}$ moment calculated for the 4^14^1 configuration than that obtained for the 4^24^0 configuration.

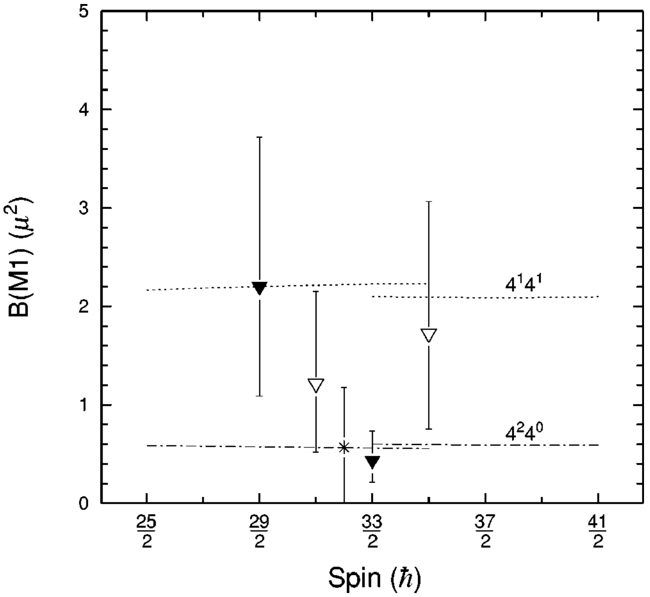

FIG. 12. $B(M1)$ values versus initial spin for the high-spin band structure in ^{57}Co extracted from measured quantities and comparison with model curves based on the Dönau-Frauendorf formalism. Filled and open triangles represent the data for bands (h) and (i), respectively. The asterisk indicates a weighted average for these data. The dotted (dash-dotted) model curves represent the calculations for the 4^14^1 (4^24^0) configuration.

The trend for the relative energies, shown in Fig. 11, also indicates the superiority of the 4^14^1 configurations in describing the bands in ^{57}Co. For the plot in Fig. 11, the experimental relative energies have been increased by 3 MeV, to put them at the same level as the HF results. That is, the absolute energies of the bands in ^{57}Co are not well reproduced by the HF calculations, but the comparison in Fig. 11 is meaningful for the spin dependence of the relative energies. In this respect, Figs. 10 and 11 consistently favor a 4^14^1 configuration assignment for the signature-partner bands in ^{57}Co.

Finally, the $M1$ properties of the two high-spin bands in ^{57}Co are discussed. From the branching ratios of Fig. 4(b) and the transition energies (in MeV), reduced transition probability $B(M1)/B(E2)$ ratios for the spin states near the bottom of the structure can be extracted according to an expression given in Ref. [26]:

$$\frac{B(M1)}{B(E2)} = 0.0693\frac{16\pi}{5}\,\frac{I_\gamma(M1)}{I_\gamma(E2)}\,\frac{E_\gamma^5(E2)}{E_\gamma^3(M1)} \quad (\mu^2/e^2\mathrm{b}^2). \tag{2}$$

Here it is assumed that the quadrupole and dipole transitions are pure $[\delta(E2/M1) = 0]$. Expression (2) together with the $B(E2)$ values for the states of interest provide a set of

$B(M1)$ values (in units of the nuclear magneton μ). The $B(E2)$ values used in this procedure are calculated according to the collective expression [27] with a constant quadrupole moment of 1.9 e b from experiment and the appropriate Clebsch-Gordan coefficients for the states in the band assuming a K quantum number of 5/2. Notice that these $B(E2)$ values are associated with errors from a proper propagation of error from the measured Q_t values.

In Fig. 12, the obtained $B(M1)$ values are shown as a function of the initial spin. Most of the uncertainties are large. The uncertainty for the data point at spin 29/2 is dominated by the error for the branching ratio, while the errors for the other points are determined mainly by the error in Q_t. Due to the large uncertainties a spin dependence of the $B(M1)$ values is not apparent. A weighted average for the $B(M1)$ values for all spins is also shown as an asterisk in Fig. 12 for further comparison with model predictions.

In order to calculate the $M1$ transition matrix elements, a formula based on the geometric model by Dönau and Frauendorf [28] is introduced:

$$B(M1)=\frac{3}{8\pi}\left[\sum_{1,\alpha}(g_{K_\alpha}-g_R)\left(\sqrt{1-\frac{K^2}{I^2}}K_\alpha-\frac{K}{I}i_\alpha\right)-\frac{K}{I}\sum_{1,\beta}(g_{i_\beta}-g_R)i_\beta\right]^2\quad(\mu^2). \tag{3}$$

This formula is a straightforward extension of the cited model which allows to perform a summation of the magnetic moments for the ‘‘deformation aligned’’ (index α) and ‘‘rotation aligned’’ (index β) components of a multiparticle multihole configuration.

The definitions of the parameters in Eq. (3) and their corresponding values are the following: For the bandhead state, $K=\Sigma_\alpha K_\alpha$ with K_α being the K quantum numbers for the individual single-particle angular momenta. The parameters i_α and i_β are the components of the individual single-particle spins along the rotational axis and their values are taken from the HF calculations. The values i_α for the ‘‘deformation aligned’’ orbitals ([303]7/2 and [312]5/2) are small ($<0.2\hbar$) and values at a low frequency ($\hbar\omega=0.1$ MeV) are taken and kept constant over the entire spin range. The alignments i_β for the ‘‘rotation aligned’’ orbitals ([440]1/2, [310]1/2, and [321]1/2) are large and values $i_\beta(I)$ are used. In the present approach, i_β is the only parameter that depends on the spin. The g factors g_{K_α} and g_{i_β} for the ‘‘deformation aligned’’ and ‘‘rotation aligned’’ orbitals are taken from a strong coupling limit estimate and from the Schmidt value [29], respectively. The g factor for the collective rotation is taken as $g_R=Z/A$. For simplicity, the signature splitting dependent ‘‘second order’’ term ($I\ \Delta e'/\hbar\omega$ [28]) has been omitted in Eq. (3).

The results for the $B(M1)$ values calculated for the 4^14^1 and 4^24^0 configurations are shown in Fig. 12 as the horizontal lines. The discontinuity at spin 33/2 reflects the configuration change (crossing) discussed above (cf. Fig. 9). The model estimates for both configurations are in the same range with the data. Given the fact that the experimental errors are large, this observation might only represent a consistency check for the two most reasonable configuration assignments selected before. However, it is remarkable that with a rather simple model and a reasonable choice of mostly constant parameters the calculated $B(M1)$ values are close to experiment.

Somewhat speculative, the mismatch between the model curves for the 4^14^1 configuration and the small $B(M1)$ value at spin 33/2, i.e., near the configuration crossing, might be due to the constant Q_t value or/and g_R factor. Indeed, at the crossing, Q_t is expected to be somewhat reduced due to a change in the core properties. At the same time, g_R might decrease since two neutron orbitals are crossing (4^14^1). For this configuration, a better fit to the data is therefore conceivable. On the other hand, assuming that there is no spin dependence in the $B(M1)$ values we may compare a weighted average of the data (Fig. 12, asterisk) with the model curves. Then, the 4^24^0 configuration appears to be in closer agreement with the data.

V. SUMMARY AND CONCLUSIONS

The presence of two rotational bands in ^{57}Co is reported and their features were described in detail. Average transition quadrupole moments were measured for these bands which show that the nuclear shape at high spin is highly deformed ($\beta_2>0.39$). The deformation of the bands in ^{57}Co is comparable with those of the bands in the neighboring Ni and Co nuclei. However, the newly observed bands in ^{57}Co are signature-partner sequences.

The features of the rotational bands in ^{57}Co were compared with results from Skyrme Hartree-Fock calculations. The calculations favor a 4^14^1 or 4^24^0 configuration assignment for the signature-partner structure, involving in either case two $1g_{9/2}$ intruder orbitals. Among these two options the 4^14^1 configuration matches the aligned spins, $\mathfrak{J}^{(2)}$ moments of inertia, and excitation energies relative to a reference versus the spin best and is therefore preferred.

The measured Q_t moments and the $B(M1)$ values for the signature-partner linking transitions were considered as another means to distinguish between the 4^14^1 and 4^24^0 configurations. However, the experimental uncertainties of these quantities are too large to favor conclusively one of the two intruder configurations. Nevertheless, the discussion of $B(M1)$ values in the present paper is the first attempt to describe the magnetic properties of signature-partner bands in the mass 60 region. Using a formula based on the Dönau-Frauendorf formalism and parameter values partially taken from the Hartree-Fock calculations, the model curves for the 4^14^1 and 4^24^0 configurations are roughly in agreement with the data.

In conclusion, with the newly observed bands in ^{57}Co the limit of the mass 60 region of deformation is shifted below the $Z=28$ shell gap. A consistent picture for particle-hole excitations across this gap involving the $1g_{9/2}$ orbital is obtained.

ACKNOWLEDGMENTS

The authors express their gratitude to the Argonne National Laboratory support staff for assistance in setting up the experiment, to D. C. Radford for making available his latest analysis software for γ-ray data, and to P. B. Semmes for valuable discussions. This work was supported by the U.S. DOE under Grant No. DE-FG02-88ER-40406, Contract Nos. DE-AC03-76SF00098 and W-31-109-ENG-38, by the Polish Committee for Scientific Research (KBN) under Contract No. 5-P03B-014-21, by a computational grant from the Interdisciplinary Centre for Mathematical and Computational Modeling (ICM) of the Warsaw University, and by the Swedish Natural Science Research Councils.

---

[1] C.E. Svensson *et al.*, Phys. Rev. Lett. **79**, 1233 (1997).
[2] D. Rudolph *et al.*, Phys. Rev. Lett. **80**, 3018 (1998).
[3] D. Rudolph *et al.*, Phys. Rev. Lett. **82**, 3763 (1999).
[4] C.E. Svensson *et al.*, Phys. Rev. Lett. **80**, 2558 (1998).
[5] T. Mizusaki, T. Otsuka, Y. Utsuno, M. Honma, and T. Sebe, Phys. Rev. C **59**, R1846 (1999).
[6] A.V. Afanasjev, I. Ragnarsson, and P. Ring, Phys. Rev. C **59**, 3166 (1999).
[7] J. Dobaczewski, W. Satuła, W. Nazarewicz, and C. Baktash (unpublished).
[8] A.V. Afanasjev, D.B. Fossan, G.J. Lane, and I. Ragnarsson, Phys. Rep. **322**, 1 (1999).
[9] W. Reviol *et al.*, Nucl. Phys. **A682**, 28c (2001).
[10] I.Y. Lee, Nucl. Phys. **A520**, 641c (1990).
[11] D. G. Sarantites *et al.* (unpublished).
[12] A new level scheme for ^{56}Co ($3pn$ channel) obtained in the course of this work will be presented in a forthcoming publication. The high-spin level scheme for ^{51}Fe ($2\alpha n$ channel) has also been established with the present setup, see J. Ekman *et al.*, Eur. Phys. J. A **9**, 13 (2000).
[13] D.G. Sarantites, P.-F. Hua, M. Devlin, L.G. Sobotka, J. Elson, J.T. Hood, D.R. LaFosse, J.E. Sarantites, and M.R. Maier, Nucl. Instrum. Methods Phys. Res. A **381**, 418 (1996).
[14] C.E. Svensson *et al.*, Nucl. Instrum. Methods Phys. Res. A **396**, 228 (1996).
[15] D.G. Sarantites, Phys. Rev. C **12**, 1176 (1975).
[16] B. Cederwall *et al.*, Nucl. Instrum. Methods Phys. Res. A **354**, 591 (1995).
[17] *Nuclear Data Sheets*, edited by M. J. Martin and J. K. Tuli (Academic, New York, 1998), Vol. 85, No. 3.
[18] C.-H. Yu *et al.*, Phys. Rev. C **62**, 041301(R) (2000).
[19] F.A. Lerma *et al.*, Phys. Rev. Lett. **83**, 5447 (1999).
[20] J. F. Ziegler, J. P. Biersack, and U. Littmark, *The Stopping and Range of Ions in Solids* (Pergamon, New York, 1985); J. F. Ziegler (private communication).
[21] D. Rudolph *et al.*, Phys. Rev. Lett. **86**, 1450 (2001).
[22] J. Dobaczewski and J. Dudek, Comput. Phys. Commun. **102**, 166 (1997); **102**, 183 (1997); **131**, 164 (2000).
[23] E. Chabanat, P. Bonche, P. Haensel, J. Meyer, and F. Schaeffer, Nucl. Phys. **A635**, 231 (1998).
[24] Figure 6 corresponds to occupying the $\nu[303]7/2(-i)$ Routhian. This state is about 1 MeV lower in energy than $\nu[303]7/2(+i)$. By reversing this occupation one obtains the reversed order of single-particle Routhians, while the total Routhians give the two (well-degenerate) sequences of signature-partner states.
[25] D. Rudolph *et al.*, Phys. Rev. C **63**, 021301(R) (2000).
[26] R.M. Lieder, A. Neskakis, J. Skalski, G. Sletten, J.D. Garrett, and J. Dudek, Nucl. Phys. **A476**, 545 (1988).
[27] A. Bohr and B. R. Mottelson, *Nuclear Structure*, (World Scientific, Singapore, 1998), Vol. II, p. 45.
[28] F. Dönau and S. Frauendorf, in *Proceedings of the International Conference on High Angular Momentum Properties of Nuclei, Oak Ridge, 1982*, edited by N. R. Johnson, (Harwood, Academic, Chur, Switzerland, 1983), Vol. 4, p. 143; F. Dönau, Nucl. Phys. **A471**, 469 (1987).
[29] The Schmidt value is calculated for a spin g factor attenuated by a factor of 0.7, an assumption that is usually made.